J Therm Anal Calorim (2012) 107:305–311
DOI 10.1007/s10973-011-1451-7

Formation of oxysulfide LnO_2S_2 and oxysulfate LnO_2SO_4 phases in the thermal decomposition process of lanthanide sulfonates (Ln = La, Sm)

Luiz Carlos Machado · Marcos Tadeu D'Orlando de Azeredo · Hamilton Perez Soares Corrêa · Jivaldo do Rosário Matos · Ítalo Odone Mazali

Received: 10 December 2010 / Accepted: 7 March 2011 / Published online: 24 March 2011

Abstract This study investigates two lanthanide compounds (La^{3+} and Sm^{3+}) obtained in water/ethyl alcohol solutions employing the anionic surfactant diphenyl-4-amine sulfonate (DAS) as ligand. Both sulfonates were characterized through IR, TG/DTG (O_2 and N_2). The thermal treatment of both compounds at 1273 K under air leaves residues containing variable percentages of lanthanide oxysulfide/oxysulfate phases shown by synchrotron high-resolution XRD pattern including the Rietveld analysis. The phase distributions found in the residues evidence the differences in the relative stability of the precursors.

Keywords Sulfonates · Thermal decomposition · Rietveld analysis

L. C. Machado (✉)
Laboratório de Produção de Novos Materiais, Departamento de Química, UFES, Av. Fernando Ferrari, 574, Vitória, ES 29075-910, Brazil
e-mail: lcmachado123@yahoo.com.br

M. T. D'Orlandode Azeredo
Laboratório de Física Aplicada, Departamento de Física, UFES, Av. Fernando Ferrari, 574, Vitória, ES 29075-910, Brazil

H. P. S. Corrêa
Laboratório de Cátalise e Cerâmicas Avançadas, UFMS, Campo Grande, Brazil

J. do Rosário Matos
Laboratório de Análise Térmica Prof. Ivo Giolito, Instituto de Química, USP, Av. Prof. Lineu Prestes 748, Bloco 8T, São Paulo, SP 05508-000, Brazil

Í. O. Mazali
Laboratório de Química do Estado Sólido, Instituto de Química, Unicamp, 6154, Campinas, SP 13084-971, Brazil

Introduction

The importance of the lighter lanthanide oxysulfate and oxysulfide systems (Ln = La, Pr, Nd and Sm) arises from their applications in semiconductors, phosphorescent material design, X-ray computerized tomography, oxygen storage, and radiation detection [1–8]. Some of these applications are based on the reversible capability of the conversion shown by lanthanide oxysulfates/oxysulfides [1–3]. Lanthanide oxysulfates ($Ln_2O_2SO_4$)/oxysulfides (Ln_2O_2S) (where Ln = La, Pr, Nd, Sm, Eu, and Gd) have been produced from the thermal decomposition of hydrated lanthanide sulfates at temperatures >1073 K for 5 h under N_2 or air [1, 8]. Subsequent reduction of as prepared $Ln_2O_2SO_4$ under a H_2 flow (3.9 mol mol^{-1}) at 1073 K leads to an oxysulfide Ln_2O_2S (Ln = La, Nd, Pr and Sm) single phase [1, 2]. The reversibility for some oxysulfides Ln_2O_2S (La, Nd and Sm) can be achieved in the temperature interval of 1073–1173 K under 2 (mol of O_2) mol^{-1}. Differently, the re-oxidation of the oxysulfide Pr_2O_2S (S^{2-}) to oxysulfate $Pr_2O_2SO_4$ (S^{6-}) occurs at temperatures <873 K [1–3]. Atypically, the thermal treatment of cerium sulfate hydrated under O_2 flow produces only the oxide [1, 2, 7, 8].

Lanthanide oxysulfides Ln_2O_2S (Ln = Sm, Eu) can also be directly obtained by thermal treatment of the oxides Ln_2O_3 at 573 K for 24 h under a flow of CS_2/Ar and low partial pressure of O_2 or also by the solid state reaction of $CuFeS_2$ with Sm_2O_3 [4, 5].

In addition, nanocrystals of EuO_2S have been produced from the thermal decomposition of Eu[(phen)–$(ddtc)_3$] (where phen = phenatroline and ddtc = diethyldithiocarbamate) using O_2 as oxidizer during the nucleation and growth process of the Eu_2O_2S nanocrystals. In the absence of protective conditions, the morphology of the Eu_2O_2S can be modulated by means of surfactant selection [6].

The direct interaction between the La^{3+} and Fe^{3+} ions and the anionic surfactant diphenyl-4-amine sulfonate (DAS) has already been studied [9, 10]. In these reactions, the metallic ions interact directly with the negative and partial charges formed by the electronic displacement inside the ligand rings toward the oxygen atoms of the sulfonate group. Under thermal treatment and atmosphere control, this effect will be sufficiently enhanced to allow the redox site S^{6+} of oxysulfate $M_2O_2SO_4$ to be reduced to S^{2-}, to give the oxysulfide M_2O_2S [1–3, 6, 9]. This effect can even achieve the reduction of Fe^{3+} in the aqueous solution [10].

Here, we compare the arrangement of the surfactant molecules around of the metallic ions Sm^{3+} and La^{3+} with the oxysulfate/oxysulfide phase distribution rate. Experimentally, the Sm^{+3} diphenylamine-4-sulfonate was produced by reaction between Sm^{3+} sulfate hydrated and Ba^{2+} diphenylamine-4-sulfonate in water/ethyl alcohol solution and characterized through IR and TG/DTG (O_2 and N_2). The La^{3+} sulfonate utilized here was previously synthesized using the ligand Na^+ diphenyl-4-amine sulfonate under the same operational conditions and also characterized through IR and TG/DTG (O_2 and N_2) [9]. Then, both the Sm^{3+} and La^{3+} sulfonates were thermally treated in the interval up to 1273 K (air flow) and their residues characterized through analysis of synchrotron high-resolution X-ray powder diffraction pattern (XRD) with Rietveld analysis to evaluate the oxysulfate/oxysulfide ($Ln_2O_2SO_4/Ln_2O_2S$) phase contents. In this study, we investigate the occurrence of the $Sm_2O_2SO_4/Sm_2O_2S$ phases in the Sm^{3+} sulfonate decomposition even though the $La_2O_2SO_4$ phase prevails after the La^{3+} sulfonate is treated at 1273 K.

Experimental procedure

Synthesis procedure of the Sm_2 $(DAS)_6{\cdot}14H_2O$

The synthesis of the Sm^{3+} diphenylamine-4-sulfonate was successful with slow addition of solutions of Sm^{3+} sulfates hydrated to the water/ethyl alcohol solutions (7:1) containing Ba-DAS. $BaSO_4$ precipitation occurred at a temperature of 343 K, under an inert atmosphere, in the absence of light and with constant agitation [9, 10].

$$Sm_2(SO_4)_3{\cdot}6H_2O_{(aq)} + 3Ba(DAS)_{2(aq)} + 8H_2O \rightarrow Sm_2(DAS)_6{\cdot}14H_2O_{(aq)} + 3BaSO_{4(s)}$$

A dark yellow product extremely soluble in water was obtained by filtration of impurities, concentration under vacuum, crystallization from and washing with purified hexane.

Characterization

Carbon, hydrogen, and nitrogen contents of the sulfonate were determined using a Perkin Elmer 2400 (CHN) analyzer. Quantitative elemental analysis of Sm^{3+} was performed by EDTA complexometric titration. The IR spectrum was obtained with a Bomem MB 100 FTIR with operation range between 350 and 4000 cm^{-1} in KBr beam splitters. Thermogravimetric analysis (TG/DTG) of the compound was carried out in a Shimadzu TGA-50H instrument, in a platinum crucible, under purified oxygen (O_2) or nitrogen (N_2) flows, at a 60 mL min^{-1} flow rate, at a temperature range of 298–1273 K (heating rate of 278 K min^{-1}). XRD diffractograms of both decomposition residues were obtained in a HZG diffractometer equipped with a quartz monochromator for the radiation line Kα of Co ($\lambda = 1.79020$ Å). The high-resolution X-ray powder diffraction (XRD) measurement was performed at the D10b-XPD beamline of the Synchrotron Light Laboratory (LNLS) using the wavelength $\lambda = 2.0836$ Å, at ambient pressure. A Ge (111) analyzer crystal was placed in a goniometer attached to the 2θ arm, and a scintillation detector was used. The Rietveld analysis was performed using the GSAS + EXPGUI suite [11–13]. The peak profile function was modeled using a convolution of the Thompson–Cox–Hastings pseudo-Voigt (pV-TCH) function14 with the asymmetry correction described by Finger et al. [15] to account for the asymmetry due to the beam axial divergence. In order to account for the anisotropy in the half width of the reflections, the bi-dimensional model described by Larson and Von Dreele [12] was used for crystallite size. For anisotropic strain, the model described by Stephens [16] was adopted.

Results and conclusions

The formula $Sm_2(DAS)_6{\cdot}14H_2O$ (% Sm exp. = 14.90, % Sm theor. = 14.74; % C exp. = 42.15, % C theor. = 42.34; % N exp. = 3.90, % N theor. = 4.11; % H exp. = 4.03, % H theor. = 4.34; yield = 60.0%; M = 2040.72 g/mol) can be assigned to the reaction product. The TG/DTG curves of the Sm^{3+} diphenyl-4-amine sulfonate under N_2 and O_2 atmospheres are presented in Figure 1a, b. The behavior of the mass loss curves under both atmospheres is significantly different. The organic losses of the Sm^{3+} diphenyl-4-amine are fully complete under O_2 at about 773 K (% residue = 25.08) (Fig. 1a), while at 1273 K under N_2 the decomposition is still incomplete (% residue = 31.54) (Fig. 1b).

The La^{3+} sulfonate was obtained as described previously by using Na^+ diphenyl-4-amine sulfonate ligand under the same conditions as the Sm^{3+} sulfonate, also

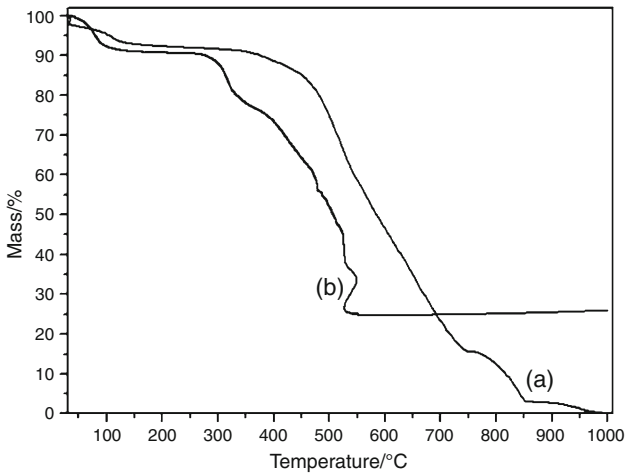

Fig. 1 TG curves of $Sm_2(DAS)_3$ under (*a*) N_2 and (*b*) O_2 flows

characterized by TG/DTG, XRD and IR data [9]. However, unlike the Sm^{3+} sulfonate synthesized in this study, the TG/DTG data for the La^{3+} sulfonate indicate total decomposition at 1273 K under N_2 (Fig. 2). The XRD of the TG residue of this compound was previously identified as the lanthanum oxide sulfate with molecular formula $La_2O_2SO_4$.

In another experiment, the La^{3+} and Sm^{3+} sulfonates were treated at 1273 K under air and both residues were then submitted to XRD analysis refined through Rietveld methodology, giving different proportions for the oxysulfate and oxysulfide phases (Table 1; Figs. 3, 4) [11–16]. The La^{3+} sulfonate residue contains the oxysulfate $La_2O_2SO_4$ as the predominant phase (83%), the LaO_2S_2 oxysulfide constitutes just a small part. Contrarily, the oxysulfide phase $Sm_2O_2S_2$ (61%) prevails in the Sm^{3+} sulfonate residue.

In both experiments described earlier, the La^{+3} sulfonate seem to present, under the same conditions, a lesser

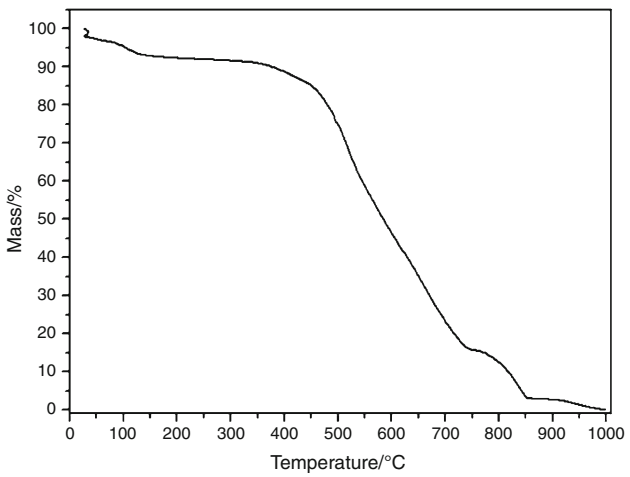

Fig. 2 TG curves for $La_2(DAS)_3$ under N_2 flow

Table 1 Oxysulfate/oxysulfide phase ratio and reliability factors evaluated by Rietveld refinement method of $Sm_2(DAS)_3$ and $La_2(DAS)_3$ decomposition products

Phases	Fractions/% mass	Reliability factors		
		Data	Sm^{3+} Phase	La^{3+} Phase
Sm_2O_2S	60.60			
$Sm_2O_2SO_4$	31.99	R_{wp}/%	15.5	27.05
Sm_2S_2O	7.41	R_p/%	12.5	17.98
La_2O_2S	16.87	R_F^2/%	1.16	2.28
$La_2O_2SO_4$	83.13	χ^2	1.733	1.233

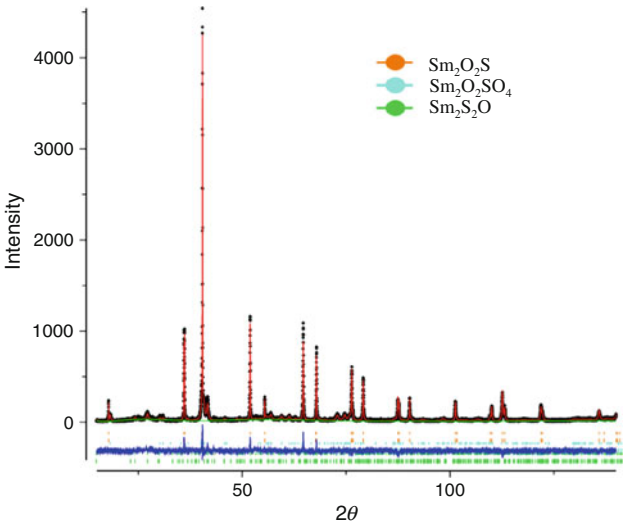

Fig. 3 X-ray powder diffraction patterns fitted using Rietveld refinement method for the product of the thermal decomposition of $Sm_2(DAS)_3$

thermal stability than the Sm^{3+} sulfonate. Normally, the lanthanide ions form compounds whose properties vary gradually together with the decrease in radius of the metal ions of the series [1–5]. However, we consider that only this effect does not seem to be enough to produce a definitive change in the sulfonate proprieties [3, 6, 9, 10]. Additional data concerning this question are presented in the following paragraphs.

The Sm^{+3} and La^{+3} sulfonates were chemically synthesized by replacing the alkaline ions [9, 10]. Therefore, some modifications in the ligand arrangements around these metal ions, more highly charged than the alkaline ions, are expected [3, 9, 10]. Table 2 contains the IR frequency assignments for Ba, La, and Sm sulfonates [9, 10, 17–21]. The IR bands of the Ba^{2+} sulfonate at frequencies of 1597, 1511, 1496 cm^{-1} are attributed to the stretching of C=C aromatic bonds in the ring. These bands were more numerous and intense in the presence of Ln^{3+} ions, that are more effective to promote the electronic

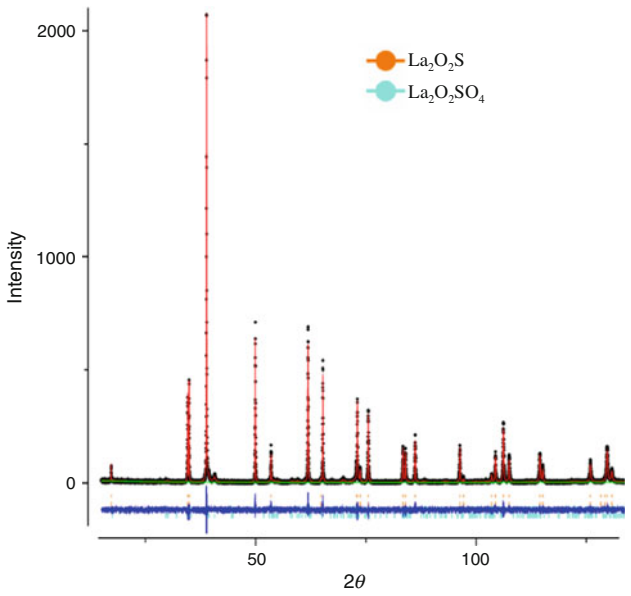

Fig. 4 X-ray powder diffraction patterns fitted using Rietveld refinement method for the product of the thermal decomposition of $La_2(DAS)_3$

Table 2 Tentative assignment of IR bands for the metal diphenyl-4-amine sulfonate (Ba^{2+}, La^{3+}, and Sm^{3+}) [9, 10, 17–21]

Tentative assignments	Band locations/cm^{-1}		
	$La_2(DAS)_3$	$Ba(DAS)_2$	$Sm_2(DAS)_3$
ν/C=C	$1593_{(s)}$	$1597_{(vs)}$	$1597_{(vs)}$
	$1520_{(sh)}$	–	$1525_{(m)}$
	$1511_{(m)}$	$1516_{(m)}$	$1513_{(m)}$
	$1494_{(vs)}$	$1496_{(vs)}$	$1494_{(m)}$
	$1450_{(vs)}$	–	$1445_{(vs)}$
δs/CH_3	$1380_{(m)}$	$1377_{(w)}$	$1375_{(m)}$
ν/C–N	–	$1325_{(w)}$	–
$\nu/(R\text{-}SO_3)^-$	–	$1229_{(sh)}$	–
	$1166_{(s)}$	$1184_{(sh)}$	$1160_{(s)}$
	$1070_{(s)}$	$1051_{(s)}$	$1037_{(s)}$
Aromatic δ/C–H aromatic	$1146_{(sh)}$	$1138_{(sh)}$	$1130_{(s)}$
	$1008_{(w)}$	$1008_{(w)}$	$1003_{(sh)}$
	$844_{(s)}$	$843_{(s)}$	$831_{(w)}$

delocalization into the diphenyl-4-amine rings. The extent of this effect can show a significant decrease in the 1326 cm^{-1} band C–N stretching. However, the torsion bands in and outside of plane of the C–H aromatic bands (1138, 1008, and 843 cm^{-1}) remain unchanged, as well as the symmetrical bending (1377 cm^{-1}) [9, 10, 17, 18, 21].

The most significant values outlined in Table 2 refer, nevertheless, to the frequency characteristics of the interaction between the sulfonate group $(SO_3)^-$ and the lanthanide ions [9, 10, 17, 18, 21]. The 1229, 1184 and 1051 cm^{-1} bands of the Ba^{+2} sulfonates can usually be attributed to the asymmetric (doubly generated) and symmetric stretching of the sulfonate group with symmetry C_{3V}. As indicated, the 1229 cm^{-1} band is strongly diminished or not found in the La^{3+} and Sm^{3+} sulfonates. This effect is usually attributed to the decrease in the C_{3V} symmetry, which removes the double degeneracy of the asymmetric stretching, lowering the group symmetry to C_{2V} [10, 17, 18, 21]. Other two bands of the Ba^{2+} sulfonate group, 1184 and 1051 cm^{-1}, were displaced to frequencies of symmetric and asymmetric stretching of the group S=O [10, 17, 18, 21]. It was previously emphasized that the modifications in the La^{3+} and Sm^{3+} environments tend to be only a gradual ligand rearrangement. Therefore, it is reasonable to suppose that the smaller Sm^{3+} ion will accommodate more easily a smaller group such as the sulfoxide (S=O). This question was previously examined [2, 3, 9, 10, 22].

The oxysulfates $Ln_2O_2SO_4$ (Ln = La, Pr) structures have been described by Rietveld analysis. The powders were similar and indexed with monoclinic structure with *C2/c* space group. The crystal structure of La and Pr oxysulfates can be described as alternative stacking of a $(Ln_2O_2)^{2+}$ layer along the a-axis interacting with the sulfate SO_4^{2-} or sulfide S^{2-} anions. The $(Ln_2O_2)^{2+}$ layers consist of tetrahedron units connected by sharing of edges [2, 3]. Nevertheless, especially for the La^{3+}oxysulfate ($Ln_2O_2SO_4$), the units of the SO_4^{2-} anion bonded to the $(La_2O_2)^{+2}$ layers show O–S–O angles in the range 104°–114° suggesting a distortion from the typical T_d symmetry [2, 3]. For the $Pr_2O_2SO_4$ structure, this distortion in the SO_4^{2-} anion symmetry is more obvious and the angles vary in the range 103°–116°. With an increase in the T_d distortion of SO_4^{-2} anion, sulfonate stability is expected to decrease. This effect is indicated as a possible structural reason for the lower reduction temperature, for the release of oxygen from $Pr_2O_2SO_4$, as well as for the unfavorable reoxidation of Pr_2O_2S to $Pr_2O_2SO_4$ [2, 3].

The structural parameters from the X-ray Rietveld method for the $La_2O_2S_2$ oxysulfide phase and $Sm_2O_2S_2$

Table 3 Crystallographic data of the La_2O_2S and Sm_2O_2S phases

Formula	La_2O_2S	Sm_2O_2S
Mol/g mol^{-1}	341.87	364.78
Crystal system	Trigonal	Trigonal
Space group	$P\bar{3}m1$ (no. 164)	$P\bar{3}m1$ (no. 164)
Cell parameters/Å	$a = 4.0512(1)$	$a = 3.8938(1)$
	$c = 6.9453(1)$	$c = 6.7163(1)$
Volume of unit cell/$Å^3$	98.71	88.19
Formula units per unit cell	1	1
Calculated density/g cm^{-3}	5.750	6.868

Table 4 Geometric parameters for La_2O_2S phase

Atomic coordinates and isotropic displacement parameters/Å^2					
Atom	Wyck	*x*	*y*	*z*	*U*
La1	2d	1/3	2/3	0.22018(19)	0.0053(3)
S1	1b	0	0	1/2	0.0015(5)
O1	2d	1/3	2/3	−0.1342(13)	0.0047(6)
Bond length/Å				Bond angle/°	
La–La	4.051(1)			La–S–La	83.53(2)
La–S	3.041(1)			S–La–S	83.53(2)
La–O	2.461(9)			S–La–O	129.72(12)

Table 5 Geometric parameters for Sm_2O_2S phase

Atomic coordinates and isotropic displacement parameters/Å^2					
Atom	Wyck	*x*	*y*	*z*	*U*
Sm1	2d	2/3	1/3	0.28037(19)	0.0091(4)
O1	2d	2/3	1/3	0.6385(15)	0.0029(6)
S1	1a	0	0	0	0.0017(6)
Bond length/Å				Bond angle/°	
Sm–Sm	3.894(1)			Sm–S–Sm	83.19(2)
Sm–S	2.933(1)			S–Sm–S	83.19(2)
Sm–O	2.405(10)			S–Sm–O	129.95(14)

phase are presented in Table 3. Both compounds can be indexed to the spatial groups P-*3ml* and the trigonal space group. The crystalline structure is also commonly described as alternative columns of $(Ln_2O_2)^{2+}$ in the tetrahedral layers connected by sharing of the edges and interacting with the S^{2-} layers. Consequently, the phase transformation from $Ln_2O_2SO_4$ to Ln_2O_2S has been considered as only involving the removal of ions surrounding sulfur as a consequence of the structural similarity between $Ln_2O_2SO_4$ and Ln_2O_2S [2, 3]. This is considered reasonable since the differences in the Ln-O_1 distance values of the La (2.461 Å), Pr (2.39 Å), and Sm (2.405 Å) oxysulfides are not really large (Tables 4, 5; Figs. 5, 6). However, despite the similarity of these values, it refers only to the effects promoted in the $(Ln_2O_2)^{2+}$ layers by the gradual decrease in the ionic radius in the lanthanide Ln^{3+} ions series [3].

Otherwise, it can be observed that the distances of La_1–S_1 = 3.041 Å and Sm_1–S_1 = 2.933 Å show significant differences which can really indicate an expressive intensification in the bond connecting the $(Sm_2O_2)^{2+}$ layers and the S^{2-} sulfide ions.

Finally, we believe that the changes in bond characteristics along the lanthanide series could reflect on the stability of oxysulfates. The structural changes in the La^{3+} ions

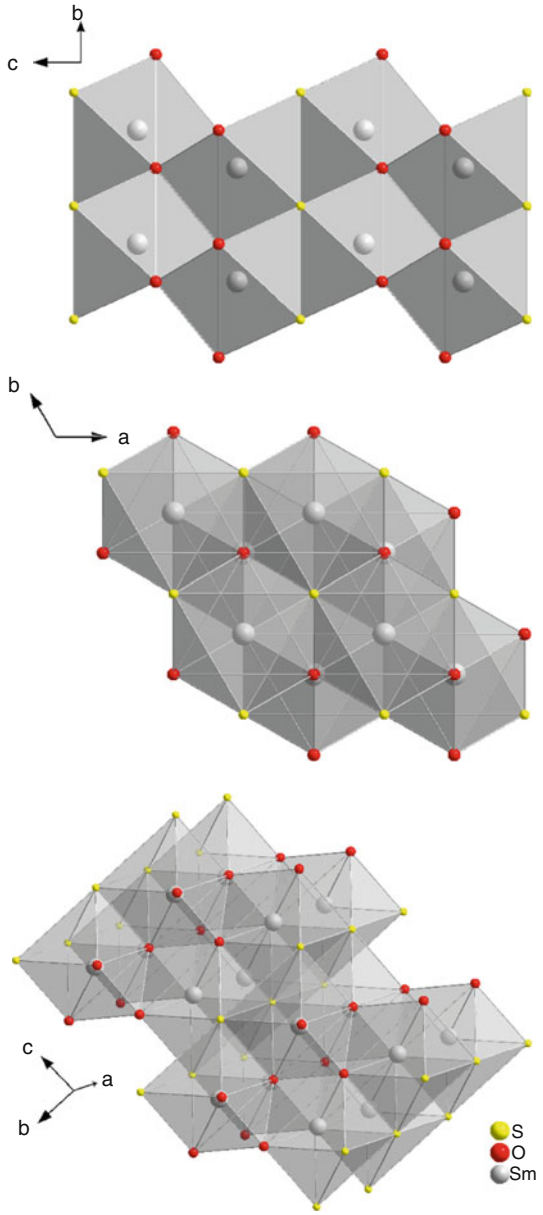

Fig. 5 Sm_2O_2S structure

symmetry when coordinated by sulfonate/oxysulfate are less hindered than during the conversion sulfonate into oxysulfide. Thus, the predominance of the La^{3+} oxysulfate over the oxysulfide phase, at 1273 K, results in a greater thermal stability for La^{3+}sulfonate. In practical terms, this behavior facilitates the understanding of the weak tendency to reduction shown by La^{3+} oxysulfate under H_2 flow [1–3].

Therefore, since the Sm^{3+} ion is smaller than La^{3+}, this ion will react more easily with the S^{2-} ions (oxysulfide) than with SO_4^{2-} ions (oxysulfate) [2, 3, 9]. For this reason, the oxysulfide phase represents the highest percentage in the thermal residue of the Sm^{3+} sulfonate at 1273 K. The conversion capacity of the oxysulfate phase into

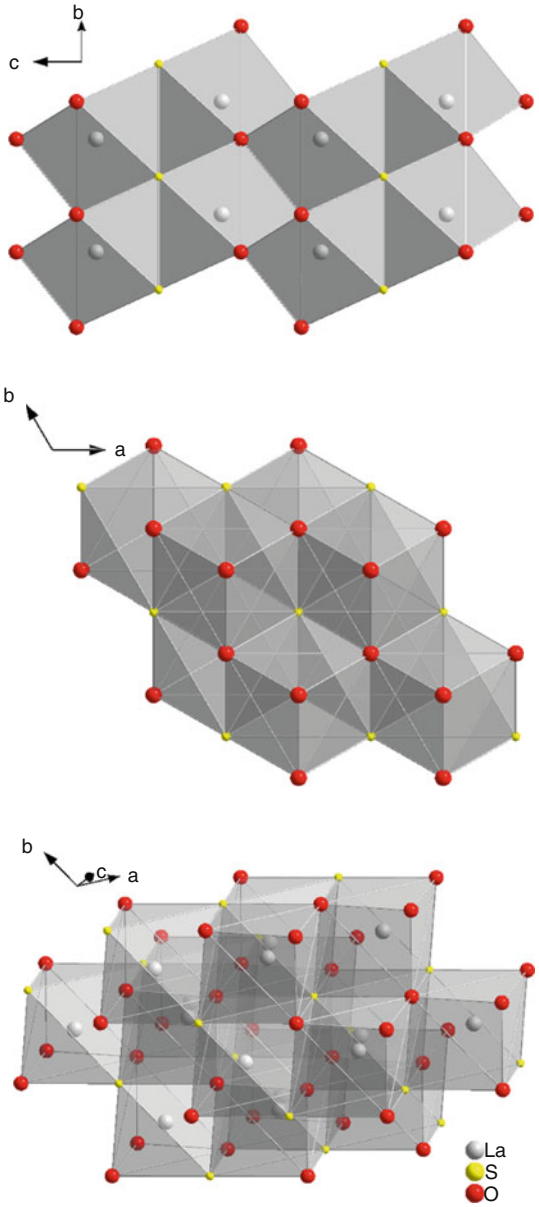

Fig. 6 La_2O_2S structure

oxysulfide is associated with the accommodation facility of the SO_4^{2-} or S^{2-} anions by the $(Ln_2O_2)^{2+}$ (Ln = La, Sm) layer. Since there are favorable interactions between the SO_4^{2-} and La^{3+}, it would tend to remain as oxysulfate. On the contrary, the Sm^{3+} accommodations will be stabilized by interactions with the sulfide anion in the C_{2v} or C_S symmetries.

Conclusions

The stability of lanthanide oxysulfides (LnO_2S) can be accentuated along the lanthanide series due to maintenance of the 3+ charge for the smallest members. The net effect of this charge is to promote the electronic displacement in the diphenyl-4-amine rings towards the oxygen bonded to the sulfur of the sulfonic group allowing the S^{6+} ions to be reduced to S^{2-} ions, leading to Ln_2O_2S. The distortion in the SO_4^{2-} group becomes stronger in the $Ln_2O_2SO_4$ containing smaller and heavier members, such as $Sm_2O_2SO_4$, thus favoring the obtainment of the Sm_2O_2S phase.

Acknowledgements We are especially grateful to the Brazilian Synchrotron Light Laboratory (LNLS) Campinas.

References

1. Machida M, Kawamura K, Ito K, Ikeue K. Large-capacity oxygen storage by lanthanide oxysulfate/oxysulfide systems. Chem Mater. 2005;17:1487–92. doi:10.1021/cm0479640.
2. Machida M, Kawano T, Eto M, Zhang D, Ikeue K. Ln dependence of the large-capacity oxygen storage/release property of Ln oxysulfate/oxysulfide systems. Chem Mater. 2007;19:954–60. doi:10.1021/cm062625n.
3. Ikeue K, Kawano T, Eto M, Zhang D, Machida M. X-ray structural study on the different redox behaviors of La and Pr oxysulfates/oxysulfides. J Alloys Compd. 2008;451:338–40. doi:10.1016/j.jallcom.2007.04.145.
4. Llanos J, Sánchez V, Mujica C, Buljan A. Synthesis, physical and optical properties, and electronic structure of the rare-earth oxysulfides Ln_2O_2S (Ln = Sm, Eu). Mater Res Bull. 2002;37:2285–91. doi:10.1016/S0025-5408(02)00936-4.
5. Llanos J, Mujica C, Henriquez A, Gómez-Romero P, Molins E. Structure refinement of samarium monothio oxide. J Alloys Compd. 2001;316:90–2. doi:10.1016/S0925-8388(00)01510-3.
6. Zhao F, Yuan M, Zhang W, Gao S. Monodisperse lanthanide oxysulfide nanocrystals. J Am Chem Soc. 2006;128:11758–9. doi:10.1021/ja0638410.
7. Casari BM, Langer V. Two $Ce(SO_4)_2{\cdot}4H_2O$ polymorphs: crystal structure and thermal behavior. J Solid State Chem. 2007;180:1616. doi:10.1016/j.jssc.2007.02.017.
8. Poston JA Jr, Siriwardane RV, Fisher EP, Miltz AL. Thermal decomposition of the rare earth sulfates of cerium(III), cerium(IV), lanthanum(III) and samarium(III). Appl Surf Sci. 2003;214:83–102. doi:10.1016/S0169-4332(03)00358-1.
9. Machado LC, Marins AAL, Muri EJB, Lacerda JAS, Balthar VO, Fulvio PF, de Freitas JCC. Reaction products between sodium diphenyl-4-amine sulfonate and hydrated $LaCl_3$: thermogravimetric and spectroscopic study. J Therm Anal Calorim. 2004;75:615–21. doi:10.1023/B:JTAN.0000027153.24401.31.
10. Machado LC, Marins AAL, Muri EJB, Biondo A, Matos JdoR, Mazali IO. Complexation of the Fe(III) and Fe(II) sulphates with diphenyl-4-amine barium sulphonate (DAS): Synthesis, thermogravimetric and spectroscopic studies. J Therm Anal Calorim. 2009;97:289–96. doi:10.1007/s10973-009-0259-1.
11. Young RA. The Rietveld method. Oxford: Oxford University Press; 1993.
12. Larson AC, Von Dreele B. General structure analysis system (GSAS) (report LAUR 86–748). Los Alamos: Los Alamos National Laboratory; 2000.
13. Toby BH. EXPGUI, a graphical user interface for GSAS. J Appl Crystallogr. 2001;34:210–3. doi:10.1107/S0021889801002242.
14. Thompson P, Cox DE, Hastings JB. Rietveld refinement of Debye-Scherrer synchrotron X-ray data from Al_2O_3. J Appl Crystallogr. 1987;20:79–83. doi:10.1107/S0021889887087090.

15. Finger LW, Cox DE, Jephcoat AP. A correction for powder diffraction peak asymmetry due to axial divergence. J Appl Crystallogr. 1994;27:892–900. doi:10.1107/S0021889894004218.
16. Stephens PW. Phenomenological model of anisotropic peak broadening in powder diffraction. J Appl Crystallogr. 1999;32:281–9. doi:10.1107/S0021889898006001.
17. Beentjes PCJ, Van Den Brand J, De Wit JHW. Interaction of ester and acid groups containing organic compounds with iron oxide surface. J Adhes Sci Technol. 2006;20:1–18. doi:10.1163/156856106775212396.
18. Zhang H, Wen X, Wang Y. Synthesis and characterization of sulfate and dodecylbenzene sulfonate intercalated zinc-iron layered double hydroxides by one-step coprecipitation. J Solid State Chem. 2007;180:1636–47. doi:10.1016/j.jssc.2007.03.016.
19. Nakanishi K, Solomon PH. Infrared absorption spectroscopy. San Francisco: Holden-Day; 1977.
20. Bellamy LJ. The infrared spectra of complex molecules. London: Chapman and Hall; 1980.
21. Braterman PS, Xu ZP. High affinity of dodecylbenzene sulfonate for layered double hydroxide and resulting morphological changes. J Mater Chem. 2003;13:268–73. doi:10.1039/B207540G.
22. Wang M, Song ZG, Jiang H, Gong H. Thermal decomposition of metal methanesulfonates in air. J Therm Anal Calorim. 2009;98:801–6. doi:10.1007/s10973-009-0119-z.